Direct Numerical Simulations of TiO 2 nanoparticle flame synthesis subjected to a homogeneous isotropic turbulent field

Y Ogata, R O Fox, Abouelmagd Abdelsamie, Dominique Thévenin, Benedetta Franzelli

Direct Numerical Simulations of TiO_2 nanoparticle flame synthesis subjected to a homogeneous isotropic turbulent field

Y. Ogata*[1], R. O. Fox[2], A. Abdelsamie[3], D. Thévenin[3], B. Franzelli[1]

[1]EM2C Laboratory, Université Paris-Saclay, CNRS, CentraleSupélec, Gif-sur-Yvette, France
[2]Department of Chemical and Biological Engineering, Iowa State University, Ames, Iowa, USA
[3]Lab. of Fluid Dynamics and Technical Flows, University of Magdeburg "Otto von Guericke", Germany

Abstract

Spray flame synthesis is a promising system for the production of nanoparticles with specific properties. For this, an accurate comprehension of the effect of turbulent flames on nanoparticle production is needed since the particle characteristics are governed by the local conditions that the particles experience along their trajectory. In this context, Direct Numerical Simulation (DNS) of academic configurations is of interest to investigate turbulence, flame and nanoparticle interactions, and to compare the performance of different models. In this work, the classical case of a flame interacting with homogeneous isotropic turbulence (HIT) is extended to TiO_2 nanoparticle flame synthesis. For this, the interaction between HIT and an H_2/air non-premixed flame, doped with titanium isopropoxide (TTIP) precursor, is considered. This configuration will allow the characterization of the evolution of particle size and morphology as functions of various simulation parameters, such as the precursor concentration and the Reynolds number of the turbulence. The role of mixing, formation, sintering, coagulation and thermophoresis can be also investigated to provide directions towards possible optimization of the aerosol systems.

Keywords: nanoparticles, direct-numerical simulation, non-premixed flames, homogeneous isotropic turbulence

Introduction

Nanoparticles can be found in a wide range of industrial applications such as healthcare and cosmetic products, food supplements, paint pigments and reinforcement catalysts [1–5]. Among diverse techniques, spray flame synthesis is a promising system for large-scale production of the final powder with controlled morphology and properties [6, 7]. However, the optimization of nanoparticle flame synthesis to produce high-quality materials requires a deep understanding of the physical processes occurring in the turbulent flame. Specifically, the final powder properties are the result of the gaseous conditions experienced by the particles during their trajectory through the flame, which are mainly governed by turbulence [1, 8]. Thus, the characterization and understanding of the multi-scale coupling between turbulence, flame, and nanoparticles are required.

For this purpose, Direct Numerical Simulation (DNS) of homogeneous isotropic turbulence (HIT) academic configurations is classically considered to investigate flame-turbulence interaction [9, 10]. The final objective of this research activity consists in extending this academic configuration to the study of TiO_2 production to understand the effect of turbulence on TiO_2 nanoparticle flame synthesis. In this work, the simplest case will be presented as a first step towards such understanding but also to propose a reference configuration that can be considered by various research groups as a starting point to evaluate and compare the performances of newly developed models. For this simplest case, combustion is still not considered and TiO_2 is already nucleated.

The remainder of the paper is structured as follows. First, the three elements constituting the configuration are presented in the most general version: turbulence, flame and nanoparticles. Then, the simplest case, here considered as the reference, will be presented together with the first results.

Numerical approaches

To investigate and constitute a canonical case towards TiO_2 flame synthesis, three major elements - turbulence, combustion and solid particles - and their roles on the multi-scale phenomena need to be identified. For this purpose, a two-dimensional square domain of size $L_x \times L_y = L^2$ is discretized by $N_x \times N_y$ points with spacing $\Delta x = \Delta y$.

Turbulence:

The turbulent gaseous field is initialized using a non-reacting decaying HIT adopting the analytical energy spectrum described by Passot and Pouquet [11]:

$$E(\kappa) = \frac{16 u_p \kappa^4}{\sqrt{\pi/2}\kappa_0^5} \exp\left(-\frac{2\kappa^2}{\kappa_0}\right) \qquad (1)$$

where u_p is the fluctuation velocity and κ_0 is the wave number at which the maximum of energy $E(\kappa)$ occurs. The turbulence level of the flow is defined by the Reynolds number $Re_t = l_t u_p/\nu$. The integral length l_t represents the largest scales of the flow with viscosity ν, while the dissipation scale is characterized by the Kolmogorov length scale η. In addition, the Taylor-scale Reynolds number $Re_\lambda = \lambda u_p/\nu$ can be used for

*Corresponding author: yuri.ogata@centralesupelec.fr

the characterization of turbulence, where λ is the Taylor length scale for the inertial subrange.

Once the initial spectrum is imposed, the calculation is run for $t = 10\tau_c$, where $\tau_c = u_p/L$ is the convective time scale and L is the domain size. This guarantees that the turbulence is fully developed. However, the turbulence also decays as physical time progresses. For a two-dimensional HIT, this can lead to a case which is not representative of a turbulent flow. The larger scales l_t should be resolved for a size three times smaller than the domain size L. In addition, the computational mesh size Δx should resolve the size at least five times smaller than the dissipation scale, guaranteeing the relation $\eta \geq 5\Delta x$.

Combustion:

The mixture in the domain needs to be initialized to characterize the combustion process. The mixture-fraction profile ψ is described using a hyperbolic tangent function in the x direction while a zero-gradient is imposed for the y direction:

$$\psi(x) = 0.5\left[1 + \tanh\left(\frac{c\,(R_d(x) - R)}{R}\right)\right] \tag{2}$$

with

$$R_d(x) = |x - 0.5L| \tag{3}$$

where $c = 3$ and $R = L/16$. The fuel mass fraction Y_f and oxidizer mass fraction Y_o are defined as follows:

$$Y_f(x) = Y_f^0\,(1 - \psi(x)) \tag{4}$$

$$Y_o(x) = Y_o^0 \psi(x) \tag{5}$$

The temperature profile $T(x)$ is imposed by computing the equilibrium temperature for the local mixture fraction following the procedure of Abdelsamie et al. [12]. The normalized fuel mass fraction $Y_f(x)/Y_f^0$ and temperature $\theta(x) = (T(x) - T_1)/(T_2 - T_1)$ are displayed in Figure 1.

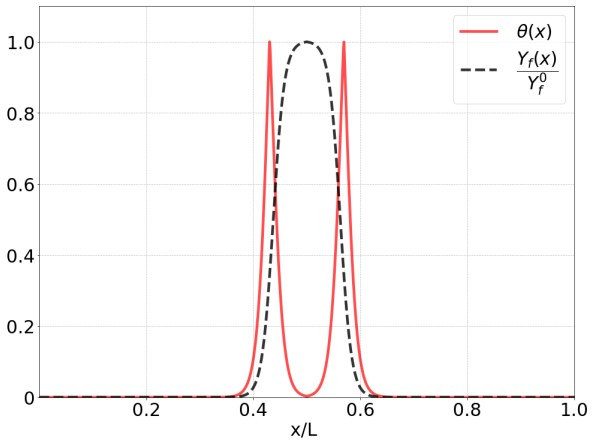

Figure 1: Initialization of fuel mass fraction and temperature profiles.

Two peaks of the temperature are observed, identifying two flame fronts. The flame thickness is then calculated using the following definition [13]:

$$\delta_L^0 = \frac{T_2 - T_1}{\max\left(\frac{\partial T}{\partial x}\right)} \tag{6}$$

The flame thickness should be resolved by at least seven points to precisely resolve chemical-reaction processes. Consequently the computational mesh of size Δx should also be chosen to guarantee $\delta_L^0 \geq 7\Delta x$.

Nanoparticle modeling:

The formation and evolution of TiO_2 are described using the monodisperse three-equation model of Kruis et al. [14], with the addition of the thermophoretic effect. The model is based on the transport of the number density N, the total surface area A, and the total volume V of the nanoparticles [15, 16]. It relies on the assumption that all aggregates have the same size with the same number of primary particles at a given location at a given time [16], i.e., a monodisperse model. The three-equations are as follows:

$$\frac{\partial N}{\partial t} + \nabla\cdot(N\mathbf{u} - D_s\nabla N) = \underbrace{-\frac{1}{2}\beta N^2}_{\text{coagulation}} + \underbrace{I}_{\text{nucleation}} \tag{7}$$

$$\frac{\partial A}{\partial t} + \nabla\cdot(A\mathbf{u} - D_s\nabla A) = \underbrace{-\frac{1}{\tau}(A - Na_s)}_{\text{sintering}} + \underbrace{Ia_0}_{\text{nucleation}} \tag{8}$$

$$\frac{\partial V}{\partial t} + \nabla\cdot(V\mathbf{u} - D_s\nabla V) = \underbrace{Iv_0}_{\text{nucleation}} \tag{9}$$

where $D_s = \nu/Sc_s$ with ν the gas viscosity and Sc_s is a constant subgrid Schmidt number. This effective diffusivity is needed to account for the fact that the nanoparticle ligaments are extremely thin so that they can not be resolved on the grid used for turbulence and combustion. Therefore, the proposed simulations will fully resolve the spatial scales of the flow and the flame but not those of the nanoparticles.

The effective velocity of the gas $\mathbf{u} = \mathbf{u_g} + \mathbf{u_T}$ considers the convection of gas flow velocity $\mathbf{u_g}$ and the thermophoresis velocity computed by $\mathbf{u_T}$. The thermophoretic velocity is driven by the fluid temperature gradient and is given by [17]:

$$\mathbf{u_T} = -C_{th}\nu\frac{\nabla T}{T} \tag{10}$$

where $C_{th} = 0.554$ [18]. The primary particle diameter d_p, the aggregate diameter d_a and the collision diameter d_c are computed as follows:

$$d_p = \frac{6V}{A} \tag{11}$$

$$d_a = \left(\frac{6V}{\pi N}\right)^{1/3} \tag{12}$$

$$d_c = d_p \left(\frac{6V}{\pi N d_p^3} \right)^{1/D_f} \tag{13}$$

where D_f is the mass fractal-like dimension for aggregates.

Three main processes - nucleation, coagulation and sintering - are considered. Nucleation is the formation of solid nuclei from gaseous precursors. The nucleation source term I can be computed differently depending on the precursor, combustion process and kinetic mechanism considered. Nucleation is then followed by coagulation and sintering processes [1].

The sintering rate determines the shape of nanoparticles, reducing the particle surface area at a constant volume and changing its fractal dimension [1, 4]. It mainly occurs in the high-temperature regions and is controlled by a characteristic sintering time τ [19].

Coagulation is the process in which two existing particles combine into a single one [1]. The coagulation kernel β defines the collision rate of the particles and is defined by [15]:

$$\beta = 4\pi d_c D \left[\frac{0.5 d_c}{d_c + g\sqrt{2}} + \frac{D\sqrt{2}}{0.5 c d_c} \right]^{-1} \tag{14}$$

The transition parameter g, length l and particle velocity c are given by

$$g = \frac{(d_c + l)^3 - \left(d_c^2 + l^2\right)^{1.5}}{3 l d_c} - d_c \tag{15}$$

$$l = \frac{8D}{\pi c} \tag{16}$$

$$c = \sqrt{\frac{8 k_b T}{\pi \rho_s V}} \tag{17}$$

where k_b is the Boltzmann constant and ρ_s is the solid particle density. To calculate the particle velocity, the particle diffusivity D is here computed using the Stokes-Einstein equation:

$$D = \frac{k_b T}{3\pi \rho_s \nu d_c} \tag{18}$$

Reference configuration

The DINO numerical code [20] is used for the present simulations. A two-dimensional domain of size $L^2 = 0.01$ m $\times$ 0.01 m with periodic boundary conditions is discretized with a computational mesh of $N_x^2 = 1024^2$ grid points. To synthesize the initial HIT, a uniform distribution of viscosity $\nu = 1.49 \times 10^{-5}$ m^2/s is imposed. Input values of 5 m/s and 2094.39 m^{-1} are chosen for u_p and κ_0, respectively, to generate the initial Passot-Pouquet spectrum. The parameters to generate the spectrum and the computational domain information are summarized in Table 1.

The characteristic time is $t_c = 2$ ms, calculated from the values of Table 1, and the simulation is ran through $t = 10\tau_c = 20$ ms to obtain fully developed turbulence.

Input parameters		Computational mesh		
u_p [m/s]	κ_0 [m^{-1}]	N_x^2	L^2 [m^2]	Δx [m]
5.0	2094.39	1024^2	0.01^2	9.76×10^{-6}

Table 1: Input parameters for energy spectrum and computational mesh information.

Figure 2 shows the energy spectrum obtained from the input parameters of Table 1 and the spectrum obtained from the simulation at $10\tau_c$. The turbulent energy dissipates due to the viscous effects, while the energy contained in the largest scales near l_t is transferred to the smaller scales η.

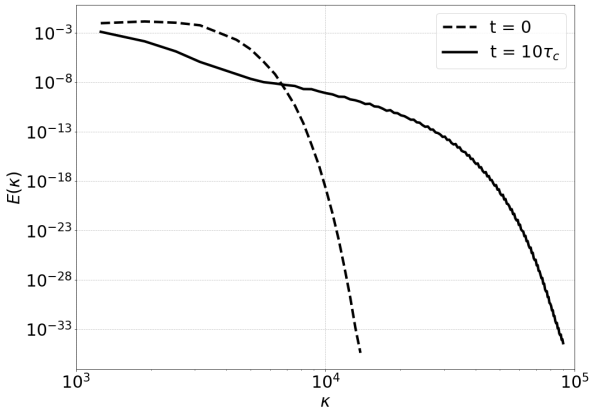

Figure 2: Energy spectrum obtained at $t = 0$ and $t = 10\tau_c$.

The properties obtained from the decaying HIT field at $t = 0$ and $t = 10\tau_c$ are displayed in Table 2. The corresponding vorticity fields are displayed in Fig. 3. At $t = 10\tau_c$, the fluctuating velocity obtained is $u_p = 3.02$ m/s and the Taylor-scale Reynolds number is $Re_\lambda = 635$. The calculated Kolmogorov scale is $\eta = 63 \times 10^{-6}$ m, while the integral scale is $l_t = 3$ mm. As a consequence, $l_t \approx 47\eta$. In Table 2, the turbulent Reynolds number is computed using $Re_t = E^{1.5} u_p / \varepsilon \nu$ where ε is the dissipation of the gaseous field.

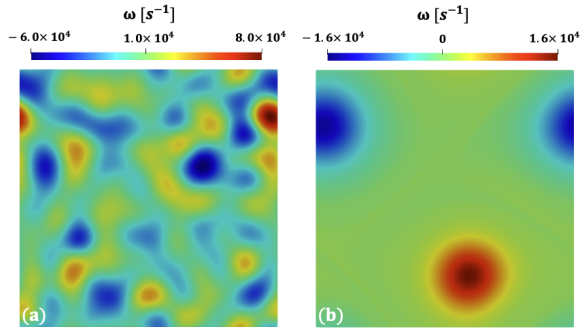

Figure 3: Instantaneous vorticity fields at (a) $t = 0$ and (b) $t = 10\tau_c$.

Two major vortices of the size of order l_t are formed as shown in Figure 3b. The largest scales obtained represent eddies three times smaller than the domain, where

t [ms]	u_p [m/s]	Re_λ	Re_t	l_t [mm]	η [m]
0	4.08	258	8208	0.985	29.8×10^{-6}
20	3.02	635	49462	3.0	63.2×10^{-6}

Table 2: Turbulence parameters obtained at $t = 0$ and $t = 10\tau_c$.

$3l_t \approx L$. In addition, the computational mesh established guarantees the description of the Kolmogorov scale encountered, using criteria $\eta \geq 5\Delta x$. The obtained instantaneous fields are superposed with the temperature and nanoparticle initial profiles, and the simulation time is reset to $t = 0$.

For the flame structure, the simplest case is considered here: chemical reactions are not activated, and only mixture fraction and temperature are computed. The mixture fraction for H_2/air is computed using $Y_f^0 = Y_{H_2}^0 = 0.056$ and $Y_o^0 = Y_{O_2}^0 = 0.23$. N_2 is added everywhere in the mixture:

$$Y_{N_2}(x) = 1 - Y_{H_2}(x) - Y_{O_2}(x) \tag{19}$$

The temperature is calculated for local species and then imposed. The maximal temperature obtained is $T_2 = 1937.8\ K$ for $Y_{H_2} = 0.019$, while the minimal temperature is $T_1 = 300$ K for $Y_{H_2} = 0$. The flame thickness obtained is then $\delta_L^0 = 0.2$ mm and it is resolved by the mesh of N_x points using the criteria defined previously.

For nanoparticles, a straightforward case is also used where TiO_2 is already nucleated. The particles initial profile is intentionally chosen to match the temperature gradient. Consequently, the peaks of the initial nanoparticle profile coincide with the maximal temperature. Pre-defined values of N, S and nanoparticles mass fraction Y_s were established as follows:

- At temperature T_2 $\begin{cases} N = 2.65 \times 10^{19}\ \text{m}^{-3} \\ S = 38.5\ \text{m}^{-1} \\ Y_s = 1.0 \times 10^{-4} \end{cases}$
- At temperature T_1 $\begin{cases} N = 0 \\ S = 0 \\ Y_s = 0 \end{cases}$

where the values for peak temperature T_2 correspond to the initial nuclei volume $v_0 = 0.16\ \text{nm}^3$ and the volume fraction $V = 4.36 \times 10^{-9}$. The initial profile of nanoparticle number density is displayed in Fig. 4.

Effect of transport and temperature

This section presents the preliminary results considering only mixing and temperature-gradient effects on the initial TiO_2 distribution. For this, sintering and coagulation are deactivated.

Figure 5 presents the instantaneous temperature at different simulated times $t = 0.24t_c$, $t = 0.5t_c$ and $t = 0.97t_c$. The two temperature fronts are initially deformed by the counter-rotating vortices. Since no reactions are activated, the combustion is not sustained and the temperature decreases with time as a result of mixing and diffusion. Eventually, the two fronts merge. The temperature front is largely deformed and wrinkled by the turbulent field. Overall, a quite homogeneous distribution of temperature is found.

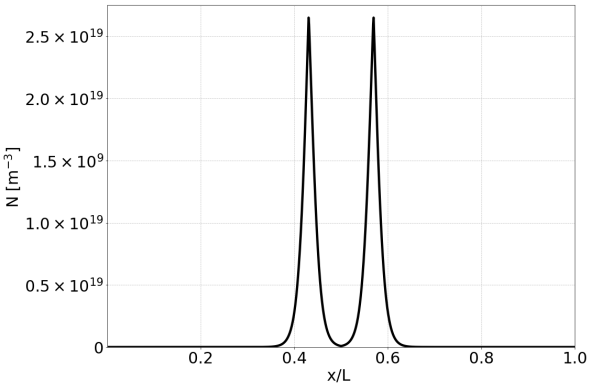

Figure 4: Initial TiO_2 number density profile.

Results for the particle number density are illustrated in Figure 6. Similarly to the temperature field, the two TiO_2 ligaments are initially deformed by the vortices. Since particle diffusivity is quite small compared to temperature, the two ligaments can be separately identified for longer computational times. In the top part of the domain, the two ligaments join due to the strain-rate effects normal to the ligaments induced by the flow. In the bottom part, the ligaments are rolled up by the vortices, where a quite inhomogeneous distribution of number density is found.

The temperature and particle number density distributions are illustrated in Figures 7 and 8, respectively, for the simulated times $t = 0$, $t = 0.24t_c$, $t = 0.5t_c$ and $t = 0.97t_c$. Cut-offs at temperature $T_c = 350$ K and nanoparticle density $N_c = 10^{16}\ \text{m}^{-3}$ are used to consider only the regions of interest. In Figure 7b, the temperature has a bimodal distribution. As thermal diffusion and convection occur, the mixture temperature converges towards a homogeneous distribution (Fig. 7c and Fig. 7d). In Figure 8, the peak of particle number density moves from higher concentrations to lower concentrations as a consequence of particle transport and thermophoresis. The maximal concentration of particles also decreases with time.

Conclusions

In this on-going work, the bases are set for DNS of TiO_2 nanoparticle synthesis subjected to homogeneous isotropic turbulence. This configuration is of interest

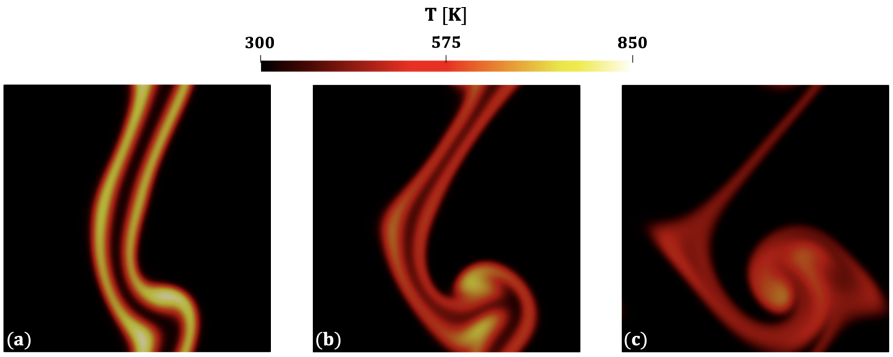

Figure 5: Instantaneous temperature fields at (a) $t = 0.24t_c$, (b) $t = 0.5t_c$ and (c) $t = 0.97t_c$.

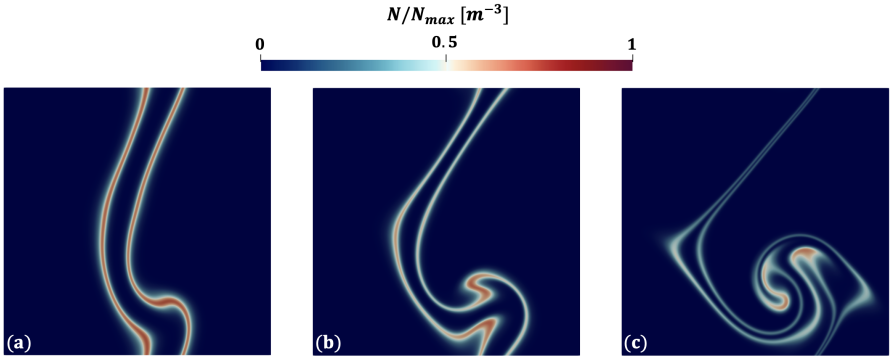

Figure 6: Instantaneous particle concentration fields at (a) $t = 0.24t_c$, (b) $t = 0.5t_c$ and (c) $t = 0.97t_c$.

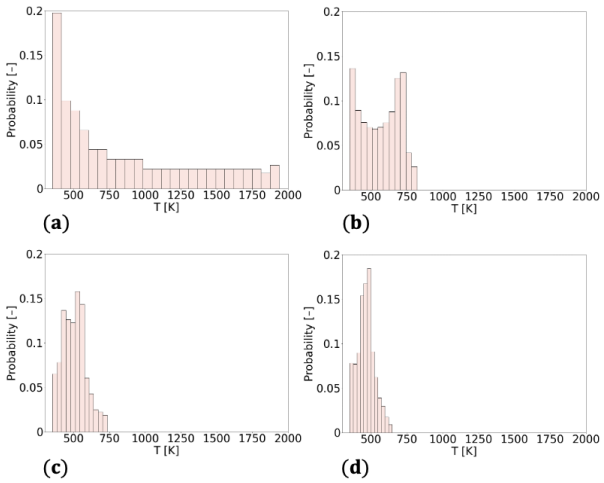

Figure 7: Temperature probability distribution at (a) $t = 0$ (b) $t = 0.24t_c$, (c) $t = 0.5t_c$ and (d) $t = 0.97t_c$.

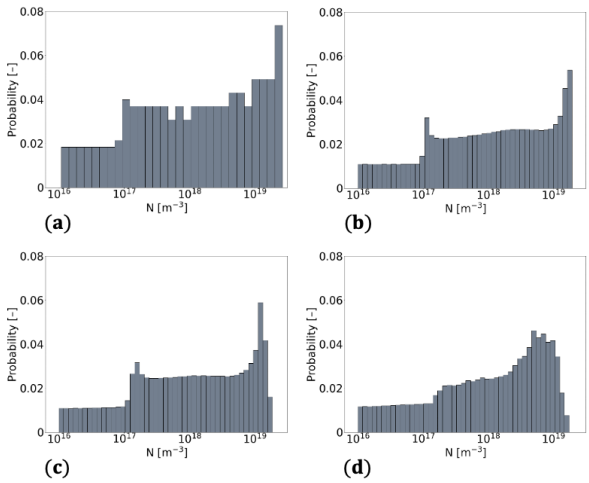

Figure 8: Particle number-density probability distribution at (a) $t = 0$ (b) $t = 0.24t_c$, (c) $t = 0.5t_c$ and (d) $t = 0.97t_c$.

to represent the interactions between the flame, turbulence and nanoparticles. A general formulation for the HIT, flame structure and the population balance equation is provided in analogy with well-established work of purely gaseous configurations. A reference case is proposed to allow the simplest relevant simulation.

First results of the temperature field and TiO_2 number density are presented as functions of time. The results illustrate the important effect of vortices and mixing on nanoparticles transport. However, diffusion and thermophoretic effect also play an important role and are still under investigation.

Although the simplest simulation is perhaps limited to represent a turbulent flow, it is a first step towards the characterization of the interactions between the flame, turbulence and nanoparticles and it can be considered easily by various research groups in order to evaluate the performances of developed models. Investigation in three-dimensional and forced HIT will complement this work in order to better characterize the ef-

fects of turbulence. For future applications, combustion and source terms will be considered to analyze TiO_2 size and morphology evolution by considering a wide range of turbulent fields at different Reynolds numbers and with different initial configurations for the non-premixed gaseous mixture. Ultimately, we wish to obtain a detailed understanding of how the flame synthesis process can be modified to achieve optimal nanoparticle properties.

Acknowledgments

This work was granted access to the HPC resources of CINES under the allocation A0112B12029 and A0132B12029 made by GENCI and of the "Mésocentre" computing center of CentraleSupélec and Ecole Normale Supérieure Paris-Saclay supported by CNRS and Région Île-de-France. This project has received the support of the European Research Council (ERC) under the European Unions' Horizon 2020 research and innovation program (grant agreement No. 757912).

References

[1] V. Raman and R. O. Fox, Modeling of fine-particle formation in turbulent flames, *Annual Review of Fluid Mechanics* **48**, 159 (2016).

[2] M. Mehta, R. O. Fox, and P. Pepiot, Reduced chemical kinetics for the modeling of TiO_2 nanoparticle synthesis in flame reactors, *Industrial & Engineering Chemistry Research* **54**, 5407—5415 (2015).

[3] M. A. Irshad, R. Nawaz, M. Z. Rehman, M. Adrees, M. Rizwan, S. Ali, S. Ahmad, and S. Tasleem, Synthesis, characterization and advanced sustainable applications of titanium dioxide nanoparticles: A review, *Ecotoxicology and Environmental Safety* **212**, 111978 (2021).

[4] M. Kraft, Modelling of particulate processes, *Powder and Particle Journal* **23**, 18 (2005).

[5] K. Wegner and S. E. Pratsinis, Scale-up of nanoparticle synthesis in diffusion flame reactors, *Chemical Engineering Science* **58**, 4581 (2003).

[6] S. E. Pratsinis, Aerosol-based technologies in nanoscale manufacturing: from functional materials to devices through core chemical engineering, *AIChE J.* **56**, 3028 (2010).

[7] G. A. Kelesidis, E. Goudeli, and S. E. Pratsinis, Flame synthesis of functional nanostructured materials and devices: Surface growth and aggregation, *Proceedings of the Combustion Institute* **36**, 29 (2017).

[8] O. I. Arabi-Katbi, S. E. Pratsinis, P. W. Morrison, and C. M. Megaridis, Monitoring the flame synthesis of TiO_2 particles by in-situ FTIR spectroscopy and thermophoretic sampling, *Combustion and Flame* **124**, 560 (2001).

[9] A. Trouve and T. Poinsot, The evolution equation for the flame surface density in turbulent premixed combustion, *Journal of Fluid Mechanics* **278**, 1 (1994).

[10] G. R. Ruetsch and M. R. Maxey, Small-scale features of vorticity and passive scalar fields in homogeneous isotropic turbulence, *Physics of Fluids A* **3**, 1587 (1991).

[11] T. Passot and A. Pouquet, Numerical simulation of compressible homogeneous flows in the turbulent regime, *Journal of Fluid Mechanics* **181**, 441 (1987).

[12] A. Abdelsamie, G. Lartigue, C. E. Frouzakis, and D. Thévenin, The Taylor–Green vortex as a benchmark for high-fidelity combustion simulations using low-Mach solvers, *Computers and Fluids* **223**, 104935 (2021).

[13] T. Poinsot and D. Veynante, *Theoretical and Numerical Combustion* (Edwards, 2011), 3rd ed.

[14] B. Scarlett, K. A. Kusters, and S. E. Pratsinis, A simple model for the evolution of the characteristics of aggregate particles undergoing coagulation and sintering, *Aerosol Science and Technology* **19**, 514 (1993).

[15] A. Abdelsamie, F. E. Kruis, H. Wiggers, and D. Thévenin, Nanoparticle formation and behavior in turbulent spray flames investigated by DNS, *Flow, Turbulence and Combustion* **105**, 497 (2020).

[16] C. Weise, J. Menser, S. A. Kaiser, A. Kempf, and I. Wlokas, Numerical investigation of the process steps in a spray flame reactor for nanoparticle synthesis, *Proceedings of the Combustion Institute* **35**, 2259 (2015).

[17] P. Rodrigues, B. Franzelli, R. Vicquelin, O. Gicquel, and N. Darabiha, Coupling an LES approach and a soot sectional model for the study of sooting turbulent non-premixed flames, *Combustion and Flame* **190**, 477 (2018).

[18] B. V. Derjaguin, A. I. Storozhilova, and Y. I. Rabinovich, Experimental verification of the theory of thermophoresis of aerosol particles, *Journal of Colloid And Interface Science* **21**, 35 (1966).

[19] B. Buesser, A. J. Gröhn, and S. E. Pratsinis, Sintering rate and mechanism of TiO_2 nanoparticles by molecular dynamics, *J. Phys. Chem. C* **115**, 11030 (2011).

[20] A. Abdelsamie, G. Fru, T. Oster, F. Dietzsch, G. Janiga, and D. Thévenin, Towards direct numerical simulations of low-Mach number turbulent reacting and two-phase flows using immersed boundaries, *Computers and Fluids* **131**, 123 (2016).